

International Federation of Automatic Control

12th IFAC Symposium on Advanced Control of Chemical Processes ADCHEM 2024

Toronto, Canada, July 14-17, 2024

PROCEEDINGS

Edited by

Martin Mönnigmann
Ruhr University Bochum, Germany
Ali Mesbah
University of California Berkeley, USA
Christopher Swartz
McMaster University, Canada



ELSEVIER

Copyright © 2024 the authors.
Open access publication under the CC-BY-NC-ND License
(<https://creativecommons.org/licenses/by-nc-nd/4.0/>)

IFAC PapersOnline — ISSN 2405-8963

Published by:
International Federation of Automatic Control (IFAC)
Hosting by Elsevier Ltd.

Available online at

www.sciencedirect.com

Publication date
July 2024

Copyright conditions

All publication material submitted for presentation at an IFAC-sponsored meeting (Congress, Symposium, Conference, Workshop) must be original and hence cannot be already published, nor can it be under review elsewhere. The authors take responsibility for the material that has been submitted. IFAC-sponsored conferences will abide by the highest standard of ethical behavior in the review process as explained on the Elsevier webpage (<https://www.elsevier.com/authors/journal-authors/policies-and-ethics>), and the authors will abide by the IFAC publication ethics guidelines (<https://www.ifac-control.org/events/organizers-guide/PublicationEthicsGuidelines.pdf/view>).

Accepted papers that have been presented at an IFAC meeting will be published in the proceedings of the event using the open-access IFAC-PapersOnLine series hosted on [ScienceDirect](https://sciencedirect.com/) (<https://sciencedirect.com/>). To this end, the author(s) must grant exclusive publishing rights to IFAC under a Creative Commons license when they submit the final version of the paper. The copyright belongs to the authors, who have the right to share the paper in the same terms allowed by the end user license, and retain all patent, trademark and other intellectual property rights (including research data).

(<https://www.ifac-control.org/publications/copyright-conditions>).

12th IFAC Symposium on Advanced Control of Chemical Processes ADCHEM 2024

Sponsored by

International Federation of Automatic Control (IFAC)
- Chemical Process Control, TC 6.1.

Co-Sponsored by

International Federation of Automatic Control (IFAC)
- TC 2.3. Non-Linear Control Systems
- TC 2.4. Optimal Control
- TC 5.2. Management and Control in Manufacturing and Logistics
- TC 6.2. Mining, Mineral and Metal Processing
- TC 6.3. Power and Energy Systems
- TC 6.4. Fault Detection, Supervision & Safety of Techn. Processes-SAFEPROCESS
- TC 8.2. Biological and Medical Systems
- TC 8.4. Biosystems and Bioprocesses

YOKOGAWA  SARTORIUS



International Programme Committee

Martin Monnigmann, DE (IPC Chair)
Ali Mesbah, US (IPC Co-Chair)
Pablo Rolandi, ES (IPC Vice-Chair from Industry)

Area Co-Chairs

Masoud Soroush, US
Boris Houska, CN
Jin Wang, US
Miroslav Fikar, SK
Mehmet Mercangöz, UK
Gabriela Henning, AR

IPC Members

Frank Allgöwer, DE
Lidia Auret, ZA
Jie Bao, AU
Don Bartusiak, US
Larry Biegler, US
Rahul Bindlish, US
Hector Budman, CA
Benoit Chachuat, UK
Cesar de Prada, ES
Denis Dochain, BE
Yining Dong, HK
Helen Durand, US
Sebastian Engell, DE
Timm Faulwasser, DE
Rolf Findeisen, DE
Martin Guay, CA
Juergen Hahn, US
Katalin Hangos, HU
Iiro Harjunkoski, FI
Hong Yue, UK
Morten Hovd, NO
Elcin Icter-Gencer, US

Marianthi Ierapetritou, US
Alf Isaksson, SE
Jamie Moreno, MX
Johannes Jäschke, NO
John Jorgensen, DK
Jay Lee, US
Sergio Lucia, DE
Adel Mhamdi, DE
Thomas Meurer, DE
Diego Munoz, CO
Masanobu Obika, JP
Sorin Olaru, FR
Leyla Özkan, NL
Radoslav Paulen, SK
Mark Pinto, US
Joe Qin, HK
Sigurd Skogestad, NO
Stefan Streif, DE
Marco Vaccari, IT
Alejandro Vargas, MX
Victor Zavala, US
Chunhui Zhao, CN

National Organizing Committee

Christopher Swartz, CA (NOC Chair)
Kim McAuley, CA (NOC Co-Chair)
Danielle Zyngier, CA (NOC Vice-Chair from Industry)

NOC Members

Carl Duchesne, CA
Sophie Felleiter, CA
Bhushan Gopaluni, CA
Biao Huang, CA

Syed Imtiaz, CA
Vinay Prasad, CA
Luis Ricardez-Sandoval, CA
Simant Upreti, CA

IFAC-PapersOnline Editorial Board

Editor-in-Chief

José-Luis Díez
Universitat Politècnica de Valencia
Spain

Advisor

Carlos Eduardo Pereira
Universidade Federal de
Rio Grande do Sul, Brazil

Editors

Systems and Signals

Alessandro Chiuso
Università di Padova, Italy

Design Methods

Laura Menini
Università di Roma "Tor Vergata",
Italy

Computer, Cognition and Communication

Thierry Marie Guerra
Université de Valenciennes et
Hainaut-Cambrésis, France

Mechatronics, Robotics and Components

Reza Moheimani
The University of Texas at Dallas,
USA

Cyber-Physical Manufacturing Enterprises

Dmitry Ivanov
Hochschule für Wirtschaft &
Recht Berlin, Germany

Process and Power Systems

Rolf Findeisen
Technische Universität
Darmstadt, Germany

Transportation and Vehicle Systems

Roberto Galeazzi
Technical University of Denmark

Bio & Ecological Systems

Ronald van Nooijen
TU Delft, Netherlands

Social Systems

Fei-Yue Wang
Chinese Academy of Sciences,
China

Associate Editors

Guillaume Mercere
Université de Poitiers, France

Tiago Roux Oliveira
Universidade Federal do Rio de
Janeiro, Brazil

Carla Seatzu
Università degli Studi di Cagliari

Yilin Mo
Tsinghua University, China

Luca Schenato
University of Padova, Italy

Sergio Galeani
Università di Roma Tor Vergata,
Italy

Elena Zattoni,
University of Bologna, Italy

Hiroshi Ito,
Kyushu Institute of Technology,
Japan

Gabriele Pannocchia
University of Pisa, Italy

Constantino Lagoa
The Pennsylvania State
University, USA

Yann Le Gorrec
ENSMM, France

Mike Barth
Karlsruhe Institute of Technology,
Germany

Kevin Guelton
Université de Reims, France

Lei Ma
Southwest Jiaotong University,
China

Wolfgang Kemmetmüller
Vienna University of Technology,
Austria

Kyoungchul Kong
Korea Advanced Institute of
Science and Technology,
Republic of Korea

Sören Hohmann
Karlsruhe Institute of Technology,
Germany

Marco Macchi
Politecnico di Milano, Italy

Fabio Sgarbossa
Norwegian University of Science
and Technology, Norway

Qing Li
Tsinghua University, China

Wei Ren
University of California, Riverside
USA

Jong Ming Lee
Seoul National University,
Republic of Korea

Chris Aldrich
Curtin University, Australia

Michela Robba
University of Genova, Italy

Vicenç Puig
Universitat Politècnica de
Catalunya, Spain

Lars Eriksson
Linköping University, Sweden

Andrea Monteriù
Università Politecnica delle
Marche, Italy

Paolo Castaldi
University of Bologna, Italy

Tankut Acarman
Galatasaray Üniversitesi, Turkey

Zdzisław Kowalczyk
Politechnika Gdańska, Poland

Timo Oksanen
Technical University Munich,
Germany

Balázs Benyó
Budapest University of
Technology and Economics,
Hungary

Marialuisa Volta
Università di Brescia, Italy

Jesus Pico i Marco
Universitat Politècnica de
Valencia, Spain

Xiao Wang
Chinese Academy of Sciences,
China

Mariana Netto
Université Gustave Eiffel, France

Xiaoyu Cao
Xi'an Jiaotong University, China

Antonio Visioli
Università di Brescia, Italy

Bahadur Ibrahimov
Azerbaijan Robotics and
Automation Society, Azerbaijan

FOREWORD

The 12th IFAC Symposium on Advanced Control of Chemical Processes (ADCHEM 2024) took place in Toronto, Canada from July 14 to July 17, 2024. The conference brought together more than 200 participants from all over the world to discuss recent developments in the control of chemical, biochemical, energy and related process systems.

The conference received 205 submissions. Based on a rigorous review process, the International Program Committee chairs selected 148 papers for presentation. The program featured 3 plenary sessions, 3 keynote sessions with a total of 6 keynote presentations, 4 invited sessions and 14 regular sessions with a total of 108 presentations, and 2 poster sessions with a total of 34 posters. The conference featured a record number of 3 half-day and 3 full-day workshops prior to the welcome reception. A panel discussion with presentations from 4 practitioners on Monday and a special industrial session spanning biopharmaceutical manufacturing, advanced materials, mineral processing and control vendor industries rounded off the scientific program. The social program consisted of a welcome reception, joint lunches and coffee breaks, the conference banquet, a closing reception, and many participants seized the opportunity to enjoy a spectacular view of Toronto from the CN Tower, for which reduced price tickets were available.

An IFAC Young Author Award was awarded at ADCHEM 2024. The winner was selected after the award committee members attended the presentations and once again closely and critically evaluated the accompanying papers. The winner of the IFAC Young Author Award was announced during the closing reception.

We would like to extend our sincere gratitude to all volunteers who helped make ADCHEM 2024 such a great success. The excellent program would not have been possible without the tremendous contributions of the National Organization Committee, the International Program Committee, the Area Chairs who each handled the reviewing process of over 30 submissions, and the numerous anonymous reviewers who helped to ensure the quality of the accepted contributions. We are also grateful for the support by our industrial sponsors and sponsoring IFAC Technical Committees. We also greatly appreciate the volunteer work and support provided by the IFAC-PapersOnLine Editorial Board.

The program of ADCHEM 2024 was interrupted by a severe power outage in the greater Toronto area on the second day of the symposium. Fortunately, the wireless network remained available, which allowed us to quickly communicate a revised schedule to all participants. After postponing the program for Tuesday afternoon by 90 minutes to give time for all organizational matters, presentations commenced without projectors using battery-powered laptops and multiple copies of presentation slides uploaded to an ad hoc server. Fortunately, power became available again after about two hours, a few minutes into the revised schedule. We thank all participants for their patience. It was great to see that a few hours of a symposium in the dark did not challenge the great team spirit of the international chemical and process control community.

Best regards,
Martin Mönnigmann (IPC Chair), Ali Mesbah (IPC Co-Chair), Chris Swartz (NOC Chair)

Model-based design of the temperature controller of a shrink tunnel

Davide Previtali* Leandro Pitturelli* Antonio Ferramosca*
Fabio Previdi*

* *Department of Management, Information and Production Engineering, University of Bergamo, Via G. Marconi 5, 24044 Dalmine (BG), Italy (e-mail: davide.previtali@unibg.it)*

Abstract: Shrink tunnels are machines composed of an industrial oven and a conveyor belt; they are widely used in manufacturing applications for polymeric packaging. Manufacturing products are wrapped in a thin plastic film and inserted into the oven via the conveyor belt. The heat shrinks the plastic around the products, creating the pack. This paper presents a model-based temperature control architecture that tackles numerous goals: setpoint tracking in the presence of manual-automatic transitions, demanding disturbance rejection requirements, energy saving, and actuator limitations. The performances of the control architecture are experimentally validated on a workbench, highlighting its effectiveness in satisfying the specifications.

Copyright © 2024 The Authors. This is an open access article under the CC BY-NC-ND license (<https://creativecommons.org/licenses/by-nc-nd/4.0/>)

Keywords: Temperature control, Black-box modelling, MIMO systems, Centralized control, PID control, Shrink tunnel.

1. INTRODUCTION

Temperature control is a vast and diverse thermal engineering field, covering applications that range from small kitchen appliances, such as convection ovens (Ryckaert et al. (1999)), to large Heating, Ventilation and Air Conditioning (HVAC) systems in buildings (Afroz et al. (2018)). Other relevant applications include: industrial furnaces (Zhang et al. (2014)), heat exchangers (Vasičkaninová et al. (2011)), heat pumps (Rastegarpour et al. (2020)), and environmental chambers (He et al. (2014)).

Designing temperature control algorithms for thermal systems can be particularly challenging for several reasons. Firstly, most plants are composed of different control zones, each with its set of actuators and sensors, making them Multiple-Input Multiple-Output (MIMO) systems. Secondly, the derivation of accurate thermal systems models is impaired by the restrictive experimental design due to the long duration of the experiments. Most often, experimental data is scarce and is the result of trials of limited duration such as step responses. Consequently, simple First Order Lag Plus time Delay (FOLPD) Transfer Function (TF) models are commonly used to describe thermal systems, see e.g. Bai et al. (2008); He et al. (2014); Ryckaert et al. (1999); Zhang et al. (2014). Lastly, several, possibly conflicting, control specifications must be satisfied. The most common are setpoint tracking, disturbance rejection, and energy saving, but there are also application-oriented goals. For example, the temperature controllers of HVAC systems must ensure a suitable level of indoor thermal comfort and minimize building energy demand while rejecting disparate disturbances, stemming from the climate, occupant behavior, and electrical grid fluctuations (Serale et al. (2018)). In the food industry, convection ovens must reach a desired target temperature (setpoint tracking) in the shortest time possible and with

negligible overshoots to meet food safety requirements and quality factors (Ryckaert et al. (1999)). Temperature uniformity within the oven cavity is also a concern. Environmental chambers share similar control specifications to convection ovens, although for different purposes (He et al. (2014)). Due to the limited complexity of the available models, control architectures based on Proportional-Integral-Derivative (PID) regulators are the most popular for thermal systems, see e.g. Bai et al. (2008); He et al. (2014); Ryckaert et al. (1999); Hu et al. (2018).

In this work, we focus on designing the temperature controllers for shrink tunnels, which are widely used in manufacturing applications for polymeric packaging. These machines are composed of an industrial convection oven and a conveyor belt that feeds products to it. The oven cavity is divided into multiple interconnected heating zones, each monitored by one or more thermocouples and with a dedicated set of heat resistors. Several convection fans favor air circulation inside the cavity. Before being inserted into the oven, the products are wrapped in a thin plastic film. The heat within the cavity shrinks the plastic and tightly envelopes the products, creating the packs. The heat resistors are connected to the electrical grid via relays, which modulate the voltages across them following the Pulse-Width Modulation (PWM) rationale. The temperature controller is responsible for producing the duty cycles of the just mentioned PWM signals. Several control specifications need to be met: (i) to maximize machine uptime, the air temperature inside the oven must reach a target temperature that is suited for the heat-shrinking process in the shortest time possible, (ii) deviations from the target temperature due to the insertion of products inside the cavity must be kept at a minimum to preserve the quality of the plastic wrapping, (iii) the downtime after machine shut down (e.g. due to possible issues on

the production line) must be mitigated by the regulator, and (iv) energy saving.

Contributions. In this paper, we focus on a shrink tunnel used in bottle packs manufacturing processes. Firstly, we derive a FOLPD model for the system under study based on experimental data. Then, we propose a model-based centralized control architecture that tackles the previously mentioned control specifications by combining several strategies from the control systems literature. The controller includes an inverted decoupler (Garrido et al. (2011)), a PI regulator for each heating zone, and a suitable Anti-Windup (AW) scheme. In particular, we extend the conditioned transfer AW algorithm in Peng et al. (1996), derived for Single Input Single Output (SISO) systems, to the MIMO case to address control actions limitations and mitigate the downtime after machine shut down. The control specifications are taken into account when calibrating the PI regulators via an ad hoc tuning rule. The performances of the proposed control architecture are experimentally validated on a shrink tunnel workbench.

Organization. The rest of this paper is organized as follows. Section 2 presents the shrink tunnel under study, whose model is described in Section 3. Then, Section 4 is devoted to the derivation of the control architecture. Its performances are experimentally validated in Section 5. Lastly, Section 6 gives some concluding remarks.

Notation. We denote by \mathbb{C} , \mathbb{R} , \mathbb{Z} , and \mathbb{N} the set of complex, real, integer, and natural numbers respectively ($0 \notin \mathbb{N}$). Given $n, m \in \mathbb{N}$, \mathbb{C}^n is the set of complex column vectors of dimension n while $\mathbb{C}^{n \times m}$ is the set of complex matrices of dimension $n \times m$. $I_n \in \mathbb{R}^{n \times n}$ is the $n \times n$ identity matrix, and $\text{diag}\{a_1, \dots, a_n\} \in \mathbb{R}^{n \times n}$ is the diagonal matrix with diagonal entries $a_1, \dots, a_n \in \mathbb{R}$. $\mathbb{R}_{>0}$ and $\mathbb{R}_{\geq 0}$ stand for the set of positive and non-negative real numbers respectively. In what follows, $t \in \mathbb{R}$ denotes the time (in s) and $f(t)$, $f: \mathbb{R} \rightarrow \mathbb{R}$, a continuous-time signal. Given a signal $f(t)$ such that $f(t) = 0, \forall t < 0$, $\mathcal{L}[f]: \mathbb{C} \rightarrow \mathbb{C}$, $F(s) = \mathcal{L}[f(t)]$, denotes the Laplace transform of $f(t)$ (Ogata (2010)). The same notation is used for vectors of signals, which are written in bold. Lastly, mod is the modulo operation.

2. SYSTEM DESCRIPTION

The schematic of the shrink tunnel under study is depicted in Fig. 1a and Fig. 1b, highlighting its main components. The industrial oven is 4.10 m long, 2.20 m tall and 1.40 m wide, while the conveyor belt is 5.70 m long. Before being inserted into the oven cavity, the bottles are mechanically grouped together and covered by a thin plastic film. An infrared sensor placed at the entrance of the oven detects when the beverages are being fed to it (see Fig. 1a). The heat shrinks the plastic and tightly envelopes the bottles, creating the packs. The oven cavity can house several bottles simultaneously and is divided into two interconnected heating zones. The heat in each zone is produced by a pair of heat resistors, located in separate compartments. The heat resistors are connected to the electrical grid via relays (one per pair of heat resistors, i.e. one per zone), which modulate the voltages across them. In particular, the relays are responsible for producing the voltage PWM signals based on the duty cycles supplied by a temperature controller. The hot air in the proximity of

the heat resistors diffuses inside the oven cavity by means of four convection fans installed at the top of the oven. The air temperature inside the oven is measured by one thermocouple per zone.

We have at our disposal a workbench that can simulate a continuous supply of beverages via an additional conveyor belt that loops around the shrink tunnel (see Fig. 1c). The signals of interest for the shrink tunnel workbench under study are ($i \in \{1, 2\}$ denotes the zone of belonging):

- The temperatures $y_i(t) \in \mathbb{R}$ (in $^\circ\text{C}$);
- The voltages across each pair of heat resistors $V_i(t) \in \mathbb{R}_{\geq 0}$ (in V), which are PWM signals with duty cycles $u_i(t) \in [0, 1]$;
- The heat flow rates $q_i(t) \in \mathbb{R}_{\geq 0}$ (in $\frac{\text{J}}{\text{s}}$) produced by the heat resistors pairs;
- The reading of the infrared sensor $d(t) \in \{0, 1\}$, which detects the presence ($d(t) = 1$) or absence ($d(t) = 0$) of bottle packs at the entrance of the oven.

The temperatures, voltages, duty cycles, and heat flow rates are grouped inside the vectors $\mathbf{y}(t) \in \mathbb{R}^2$, $\mathbf{V}(t) \in \mathbb{R}_{\geq 0}^2$, $\mathbf{u}(t) \in [0, 1]^2$, and $\mathbf{q}(t) \in \mathbb{R}_{\geq 0}^2$ respectively.

3. SHRINK TUNNEL MODELLING AND IDENTIFICATION

In this Section, we derive a control-oriented model for the shrink tunnel under study. Fig. 2 depicts the block diagram of the system. We assume that the overall temperatures within the oven cavity are the sum of three contributions: $\mathbf{y}'(t) \in \mathbb{R}^2$, $\mathbf{y}''(t) \in \mathbb{R}^2$, and $\mathbf{y}'''(t) \in \mathbb{R}$, i.e.

$$\begin{aligned} \mathbf{Y}(s) &= \mathbf{Y}'(s) + \mathbf{Y}''(s) + [1 \ 1]^\top \cdot \mathbf{Y}'''(s) \\ &= \mathbf{G}(s) \cdot \mathbf{U}(s) + \mathbf{H}(s) \cdot D(s) + [1 \ 1]^\top \cdot \mathbf{Y}'''(s). \end{aligned} \quad (1)$$

The first term originates from the heat produced by the heat resistors (which depends on the duty cycles $\mathbf{u}(t)$), the second stems from the flow of bottle packs $d(t)$, the third one is the ambient temperature $\mathbf{y}'''(t)$. In what follows, we derive a TF matrix $\mathbf{G}(s) \in \mathbb{C}^{2 \times 2}$ describing the relationship between $\mathbf{u}(t)$ and $\mathbf{y}(t)$. The derivation of the TF matrix $\mathbf{H}(s) \in \mathbb{C}^2$ is out of scope of this paper.

Shrink tunnel modelling. The heat flow rates $q_i(t)$ produced by the heat resistor pairs depend on the square of the voltages across them $V_i(t)$ according to:

$$q_i(t) = R_{\text{heat}}^{-1} \cdot V_i(t)^2, \quad i \in \{1, 2\}, \quad (2)$$

where $R_{\text{heat}} \in \mathbb{R}_{>0}$ (in Ω) is the resistance of a pair of heat resistors. In particular, the voltages are PWM signals with duty cycles $u_i(t)$ and period $T_P \in \mathbb{R}_{>0}$, $T_P = 1$ s. Let $k \in \mathbb{Z}$ be the PWM time interval index such that the k -th interval is defined as:

$$\mathcal{I}_k = \left[k \cdot T_P, (k+1) \cdot T_P \right). \quad (3)$$

By definition, $u_i(t)$ are piecewise constant signals since

$$u_i(t) = u_i(k \cdot T_P), \quad \forall t \in \mathcal{I}_k, k \in \mathbb{Z}, \quad (4)$$

holds, i.e. the duty cycles cannot change during a PWM interval. The corresponding voltage signals read as:

$$V_i(t) = \begin{cases} V_g & \text{if } k \cdot T_P \leq t < [k + u_i(t)] \cdot T_P \\ 0 & \text{if } [k + u_i(t)] \cdot T_P \leq t < [k + 1] \cdot T_P \end{cases}, \quad (5)$$

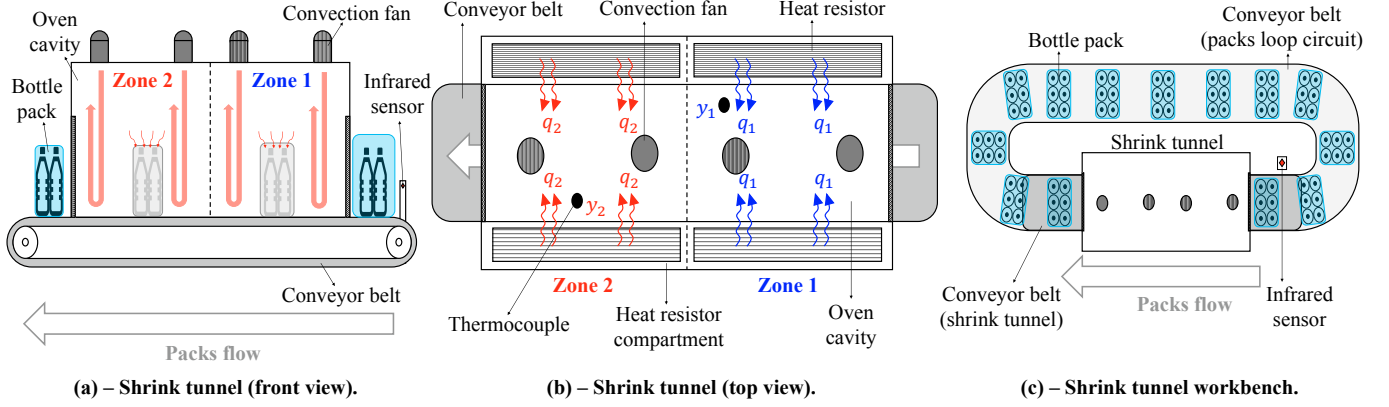


Fig. 1. Schematic of the considered shrink tunnel and of the workbench at our disposal.

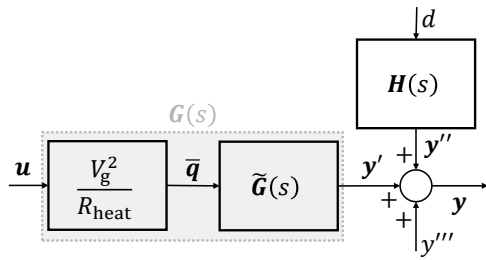


Fig. 2. Block diagram of the shrink tunnel under study.

where $V_g \in \mathbb{R}_{>0}$ (in V) is the grid voltage, which is (roughly) constant during normal operation of the shrink tunnel. Given that the PWM period T_P (1 s) is notably smaller than the time constants associated with the heating and cooling dynamics (which are in the order of minutes) due to the high thermal inertia of the oven, we consider the average heat flow rates $\bar{q}_i(t)$ for each PWM interval rather than the instantaneous rates $q_i(t)$:

$$\begin{aligned} \bar{q}_i(t) &= \frac{1}{T_P} \cdot \int_{k \cdot T_P}^{(k+1) \cdot T_P} q_i(\tau) d\tau, \quad \forall t \in \mathcal{I}_k, k \in \mathbb{Z} \\ &= R_{\text{heat}}^{-1} \cdot V_g^2 \cdot u_i(k \cdot T_P) = R_{\text{heat}}^{-1} \cdot V_g^2 \cdot u_i(t). \end{aligned} \quad (6)$$

Adapting from the temperature control literature reviewed in Section 1, we model the relationship between the average heat flow rates $\bar{q}_j(t)$, $j \in \{1, 2\}$, and the temperatures $y'_i(t)$, $i \in \{1, 2\}$, using a FOLPD TF $\tilde{G}_{ij}(s) \in \mathbb{C}$:

$$Y'_i(s) = \tilde{G}_{ij}(s) \cdot \bar{Q}_j(s), \quad \tilde{G}_{ij}(s) = \frac{\tilde{\mu}_{ij}}{1 + s \cdot \tau_{ij}} \cdot e^{-s \cdot \gamma_{ij}},$$

where $\tilde{\mu}_{ij} \in \mathbb{R}_{>0}$ (in $\frac{^\circ\text{C} \cdot \text{s}}{\text{J}}$) is the gain, $\tau_{ij} \in \mathbb{R}_{>0}$ (in s) is the time constant, and $\gamma_{ij} \in \mathbb{R}_{>0}$ (in s) is the time delay. Due to the linearity of the Laplace transform (Ogata (2010)) and (6), $\bar{Q}_j(s) = R_{\text{heat}}^{-1} \cdot V_g^2 \cdot U_j(s)$, leading to:

$$Y'_i(s) = G_{ij}(s) \cdot U_j(s), \quad G_{ij}(s) = \frac{\mu_{ij}}{1 + s \cdot \tau_{ij}} \cdot e^{-s \cdot \gamma_{ij}}, \quad (7)$$

where $\mu_{ij} = \tilde{\mu}_{ij} \cdot R_{\text{heat}}^{-1} \cdot V_g^2$ (in $^\circ\text{C}$). Consequently, the TF matrix $\mathbf{G}(s)$ in (1) is given by:

$$\mathbf{G}(s) = \begin{bmatrix} G_{11}(s) & G_{12}(s) \\ G_{21}(s) & G_{22}(s) \end{bmatrix}. \quad (8)$$

Identification. The parameters of the TFs $G_{ij}(s)$, $i, j \in \{1, 2\}$, in (7) are estimated via open-loop experiments. Due to the long duration of the trials, we resort to two step

Table 1. Estimated parameters for the transfer functions $G_{ij}(s)$ in (7).

i	j	μ_{ij} [$^\circ\text{C}$]	τ_{ij} [s]	γ_{ij} [s]	Fit [%]
1	1	192.3	841.7	110.9	95.3%
1	2	59.3	1315.9	162.4	95.1%
2	1	92.5	1218.4	133.1	96.5%
2	2	111.6	757.1	14.3	91.0%

response tests. In the first experiment, we set the duty cycle of the heat resistors in zone 1 to $u_1(t) = 0.6, \forall t \geq 0$, while the heat resistors of zone 2 are kept off (i.e. $u_2(t) = 0, \forall t \in \mathbb{R}$). Vice versa for the second experiment in which $u_1(t) = 0, \forall t \in \mathbb{R}$, and $u_2(t) = 0.6, \forall t \geq 0$. In both trials no bottle packs are inserted inside the oven. The ambient temperature is roughly constant, playing no role in the identification. We estimate $\mu_{ij}, \tau_{ij}, \gamma_{ij}$ for $G_{ij}(s)$, $i, j \in \{1, 2\}$, following the output-error approach (Verhaegen and Verdult (2007)). Table 1 reports the estimated parameters and the fits computed as $1 - \text{NRMSE}$ (Normalized Root Mean Square Error).

4. CONTROL ARCHITECTURE

In this Section, we propose a control architecture for the shrink tunnel under study. The heat-shrinking process works as follows. The air temperature inside the oven must be kept at a desired value that allows the plastic film wrapped around the bottles to shrink uniformly during the pack travel time inside the cavity (see Fig. 1a). The target temperatures range from 120°C to 200°C , depending vastly on the installed plastic film, the processed beverages, and the airflow inside the oven cavity. In any case, the beverages are inserted inside the oven only when the target temperature is reached; any deviance from the desired temperature must be kept at a minimum during the heat-shrinking process to prevent quality degradation of the wrapping. Thus, the main control specifications are:

- (S.1) The temperatures $y_i(t)$, $i \in \{1, 2\}$, must track piecewise constant setpoints $\text{SP}_i(t) \in \mathbb{R}$ (in $^\circ\text{C}$). When started from the ambient temperature, the $y_i(t)$'s must reach the target temperatures within 35 min. Instead, low-to-moderate setpoint changes ($10 \div 20^\circ\text{C}$ differences) must be handled within 20 min. This specification maximizes machine uptime.
- (S.2) Disturbance rejection. Deviations from the target temperatures must be kept within a $\pm 5^\circ\text{C}$ tolerance

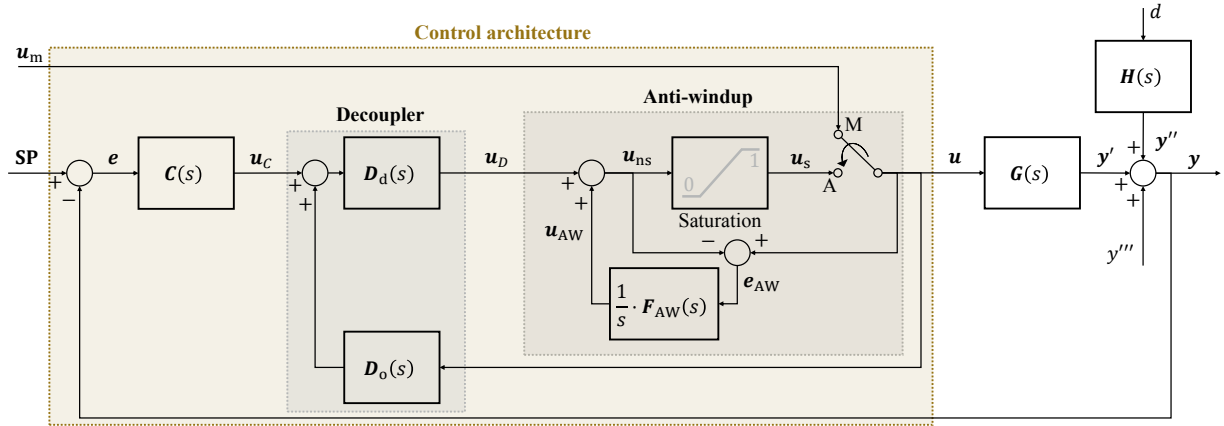


Fig. 3. Block diagram of the control architecture for the shrink tunnel under study.

during the heat-shrinking process. Failing to meet this specification for several minutes may impact the quality of the wrapping.

(S.3) The shrink tunnel is subject to several manual-automatic transitions during operation. Whenever there is any problem with the production line, the machine is shut down until it is solved. A shut down can be seen as switching the machine to manual mode by setting $u_i(t) = 0$ and $SP_i(t) = 0^\circ\text{C}$, $i \in \{1, 2\}$, temporarily. When the production line is restarted, the temperatures must converge to the setpoints in the shortest time possible, mitigating machine downtime.

(S.4) Energy saving. The controller should minimize the energy consumption of the heat resistors, which is given by (stemming from (4) and (5)):

$$\sum_{i=1}^2 \int_0^{t_{\text{end}}} \frac{V_i(\tau)^2}{R_{\text{heat}}} d\tau = \sum_{i=1}^2 \sum_{k=0}^{\frac{t_{\text{end}}}{T_P} - 1} \frac{V_g^2 \cdot T_P}{R_{\text{heat}}} \cdot u_i(k \cdot T_P), \quad (9)$$

where $t = 0$ is the time instant at which the shrink tunnel is turned on and $t = t_{\text{end}}$, $t_{\text{end}} \in \mathbb{R}_{>0}$, when it is stopped, assuming $t_{\text{end}} \bmod T_P = 0$.

(S.5) The control actions $u_i(t)$, $i \in \{1, 2\}$, must be between 0 and 1 (saturation).

Due to the MIMO nature of the shrink tunnel, we propose a centralized control architecture based on an inverted decoupler (Garrido et al. (2011)). The temperature in each zone is controlled by a PI regulator, whose tuning is eased by the presence of the decoupler and done according to (S.1) and (S.4). To minimize (9), the controller should produce smooth control actions. Disturbance rejection is intrinsically performed by the regulator, given its closed-loop nature. Thus, we will check experimentally (a-posteriori) if (S.2) is satisfied (see Section 5). The saturation of the duty cycles in (S.5) is handled via conditioned transfer anti-windup (Peng et al. (1996)), which also maximizes the setpoint tracking performances after manual-automatic transitions (covering (S.3) as well). The resulting control architecture is depicted in Fig. 3, where $\mathbf{SP}(t) = [SP_1(t) \ SP_2(t)]^\top \in \mathbb{R}^2$ is the setpoint vector, and $\mathbf{u}_m(t) = [u_{m_1}(t) \ u_{m_2}(t)]^\top \in [0, 1]^2$ are the manual control actions, see (S.3). In the control architecture, the saturation block works component-wise and as follows:

$$u_{s_i}(t) = \max \left\{ \min \{u_{ns_i}(t), 1\}, 0 \right\}, \quad i \in \{1, 2\}. \quad (10)$$

$\mathbf{u}_s(t) = [u_{s_1}(t) \ u_{s_2}(t)]^\top \in [0, 1]^2$ are the limited control actions, while $\mathbf{u}_{ns}(t) = [u_{ns_1}(t) \ u_{ns_2}(t)]^\top \in \mathbb{R}^2$ are those before saturation. The switch denotes which duty cycles should pass through in the block diagram when the system operates in Manual (M) or Automatic (A) mode.

Inverted decoupler. Consider the block diagram in Fig. 3. The decoupled control actions $\mathbf{u}_D(t) = [u_{D_1}(t) \ u_{D_2}(t)]^\top \in \mathbb{R}^2$ are given by:

$$\mathbf{U}_D(s) = \mathbf{D}_d(s) \cdot [\mathbf{U}_C(s) + \mathbf{D}_o(s) \cdot \mathbf{U}(s)], \quad (11)$$

where $\mathbf{u}_C(t) = [u_{C_1}(t) \ u_{C_2}(t)]^\top \in \mathbb{R}^2$ are the control actions produced by the PI regulators described by the TF matrix $\mathbf{C}(s) \in \mathbb{C}^{2 \times 2}$. Let us assume that the system always operates in automatic mode and no saturations take place. Then, $\mathbf{u}(t) = \mathbf{u}_D(t)$ and (11) reduces to $\mathbf{U}_D(s) = \mathbf{D}_{\text{inv}}(s) \cdot \mathbf{U}_C(s)$ with $\mathbf{D}_{\text{inv}}(s) \in \mathbb{C}^{2 \times 2}$,

$$\mathbf{D}_{\text{inv}}(s) = [\mathbf{I}_2 - \mathbf{D}_d(s) \cdot \mathbf{D}_o(s)]^{-1} \cdot \mathbf{D}_d(s), \quad (12)$$

being the inverted decoupler TF matrix. By setting:

$$\mathbf{D}_d(s) = \mathbf{I}_2, \quad \mathbf{D}_o(s) = \begin{bmatrix} 0 & -\frac{G_{12}(s)}{G_{11}(s)} \\ -\frac{G_{21}(s)}{G_{22}(s)} & 0 \end{bmatrix}, \quad (13)$$

it is possible to prove that the loop TF matrix $\mathbf{L}(s) \in \mathbb{C}^{2 \times 2}$ amounts to (Garrido et al. (2011)):

$$\begin{aligned} \mathbf{L}(s) &= \mathbf{G}(s) \cdot \mathbf{D}_{\text{inv}}(s) \cdot \mathbf{C}(s) \\ &= \text{diag} \{G_{11}(s), G_{22}(s)\} \cdot \mathbf{C}(s). \end{aligned} \quad (14)$$

Given that, from a frequency response perspective, $\tau_{11} \approx \tau_{12}$ and $\tau_{22} \approx \tau_{21}$ (see Table 1), we can make the following approximations in (13):

$G_{12}(s) \cdot G_{11}(s)^{-1} \approx \mu_{12} \cdot \mu_{11}^{-1}$, $G_{21}(s) \cdot G_{22}(s)^{-1} \approx \mu_{21} \cdot \mu_{22}^{-1}$, resulting in a static decoupler.

PI controllers. Due to the centralized control architecture, we design a diagonal PI controller TF matrix:

$$\mathbf{C}(s) = \text{diag} \{C_1(s), C_2(s)\}, \quad C_i(s) = \frac{K_{P_i} \cdot (1 + s \cdot T_{I_i})}{T_{I_i} \cdot s}, \quad (15)$$

where $K_{P_i} \in \mathbb{R}$ (in $\frac{1}{\text{C}}$) and $T_{I_i} \in \mathbb{R}$ (in s), $i \in \{1, 2\}$, are the proportional gain and integral time constant respectively. Given that (14) holds approximately, when no saturations take place, under (15) the loop TF matrix

amounts to:

$$\mathbf{L}(s) \approx \text{diag}\{L_1(s), L_2(s)\}, \quad L_i(s) \approx G_{ii}(s) \cdot C_i(s). \quad (16)$$

Then, we can design each control loop independently, following traditional loop shaping rules (Ogata (2010)). We propose a simple model-based PI tuning rule to meet (S.1) and (S.4). By setting $T_{I_i} = \tau_{ii}$, the loop TFs in (16) amount to:

$$L_i(s) \approx K_{P_i} \cdot \frac{\mu_{ii}}{\tau_{ii}} \cdot \frac{1}{s} \cdot e^{-s \cdot \gamma_{ii}}.$$

We can easily derive the gain crossover frequency $\omega_{c_i} \in \mathbb{R}_{\geq 0}$ (in $\frac{\text{rad}}{\text{s}}$) and the phase margin $\varphi_{m_i} \in \mathbb{R}$ (in $^\circ$) for each control loop (Ogata (2010)):

$$\omega_{c_i}(K_{P_i}) \approx K_{P_i} \cdot \frac{\mu_{ii}}{\tau_{ii}}, \quad (17a)$$

$$\varphi_{m_i}(K_{P_i}) \approx 90^\circ - K_{P_i} \cdot \frac{180^\circ}{\pi} \cdot \frac{\mu_{ii} \cdot \gamma_{ii}}{\tau_{ii}}, \quad (17b)$$

which depend linearly on K_{P_i} . (S.1) boils down to maximizing the gain crossover frequency since $\omega_{c_i}(K_{P_i})$ is an approximation of the frequency of the dominant pole of the closed-loop system (Ogata (2010)). Assuming that the system operates in the linear region (no saturations), the settling time of $y_i(t)$ after a step change in $\text{SP}_i(t)$ is roughly equal to (Ogata (2010)):

$$\sigma_i(K_{P_i}) \approx 4.6 \cdot \omega_{c_i}(K_{P_i})^{-1} \quad [\text{s}]. \quad (18)$$

We propose to tune the proportional gains K_{P_i} of the controllers by solving the following Linear Programs (LPs):

$$\arg \max_{K_{P_i}} \omega_{c_i}(K_{P_i}), \quad i \in \{1, 2\} \quad (19)$$

$$\text{s.t. } \omega_{c_i}(K_{P_i}) \leq \omega_{c_{\max}}, \quad \varphi_{m_i}(K_{P_i}) \geq \varphi_{m_{\min}}.$$

$\omega_{c_{\max}} \in \mathbb{R}_{\geq 0}$ (in $\frac{\text{rad}}{\text{s}}$) is a maximum gain crossover frequency that prevents unnecessary high K_{P_i} 's that can be chosen to meet (S.1) according to (18). For example, we could choose a minimum settling time $\sigma_{\min} \in \mathbb{R}_{>0}$ (in s) and set $\omega_{c_{\max}} = 4.6 \cdot \sigma_{\min}^{-1}$. Instead, $\varphi_{m_{\min}} \in [30^\circ, 80^\circ]$ is a minimum phase margin, set in a conservative range, which avoids excessive oscillations in $\mathbf{y}(t)$ and guarantees closed-loop stability of the system. High $\varphi_{m_{\min}}$ favor low PI gains, leading to smooth control actions and energy saving. In practice, the constraints in (19) are both upper bounds on K_{P_i} . Then, the solutions of the LPs in (19) are:

$$K_{P_i} = \min \left\{ \omega_{c_{\max}} \cdot \frac{\tau_{ii}}{\mu_{ii}} (90^\circ - \varphi_{m_{\min}}) \cdot \frac{\pi}{180^\circ} \cdot \frac{\tau_{ii}}{\mu_{ii} \cdot \gamma_{ii}} \right\}. \quad (20)$$

Anti-windup scheme. To tackle (S.3) and (S.5), we extend the conditioned transfer anti-windup algorithm described in Peng et al. (1996), which only covered the SISO case, to the proposed MIMO control architecture. In what follows, we sketch the proof demonstrating that, by choosing the AW TF matrix $\mathbf{F}_{\text{AW}}(s) \in \mathbb{C}^{2 \times 2}$ as:

$$\mathbf{F}_{\text{AW}}(s) = \text{diag}\{T_{I_1}^{-1}, T_{I_2}^{-1}\}, \quad (21)$$

the tracking performances after manual-automatic transitions are maximized. In Fig. 3, $\mathbf{y}(t)$, $\mathbf{u}_{\text{ns}}(t)$, and $\mathbf{u}(t)$ are linked by:

$$\mathbf{Y}(s) = \mathbf{SP}(s) - \mathbf{W}(s) \cdot \mathbf{U}_{\text{ns}}(s) + \mathbf{C}(s)^{-1} \cdot \mathbf{D}_d(s)^{-1} \cdot \left[\mathbf{D}_d(s) \cdot \mathbf{D}_o(s) + \frac{1}{s} \cdot \mathbf{F}_{\text{AW}}(s) \right] \cdot \mathbf{U}(s), \quad (22)$$

$$\mathbf{W}(s) = \mathbf{C}(s)^{-1} \cdot \mathbf{D}_d(s)^{-1} \cdot \left[\mathbf{I}_2 + \frac{1}{s} \cdot \mathbf{F}_{\text{AW}}(s) \right].$$

We define the realizable reference vector $\mathbf{SPR}(t) \in \mathbb{R}^2$ as the setpoint vector such that if it had been applied instead of $\mathbf{SP}(t)$, the control actions before saturation, i.e. $\mathbf{u}_{\text{ns}}(t)$, would have been equal to the actual inputs $\mathbf{u}(t)$ obtained with the reference $\mathbf{SP}(t)$, without any saturation taking place. The same concept applies if manual control actions $\mathbf{u}_m(t)$ were applied instead of the ones computed by the controller. Analogously to the derivation in Peng et al. (1996) (this time in the MIMO case), by setting $\mathbf{u}(t) = \mathbf{u}_{\text{ns}}(t)$ in (22), we obtain the following expression for the realizable reference vector:

$$\mathbf{SPR}(s) = \mathbf{Y}(s) + \mathbf{C}(s)^{-1} \cdot \left[\mathbf{D}_d(s)^{-1} - \mathbf{D}_o(s) \right] \cdot \mathbf{U}(s). \quad (23)$$

Due to the definition of realizable reference, the outputs $\mathbf{y}(t)$ in (22) should match the outputs that we would obtain by applying $\mathbf{SPR}(t)$ in (23) instead of $\mathbf{SP}(t)$ (starting from the same initial conditions). Then, we can substitute $\mathbf{Y}(s)$ in (23) with (22), leading to:

$$\mathbf{SPR}(s) = \mathbf{SP}(s) + \mathbf{W}(s) \cdot [\mathbf{U}(s) - \mathbf{U}_{\text{ns}}(s)]. \quad (24)$$

By setting $\mathbf{F}_{\text{AW}}(s)$ as in (21), under (13) and (15), it is possible to prove that, in the time-domain, component-wise, (24) amounts to:

$$\text{SPR}_i(t) = \text{SP}_i(t) + K_{P_i}^{-1} \cdot [u_i(t) - u_{\text{ns}_i}(t)], \quad i \in \{1, 2\}.$$

Therefore, once $u_i(t) = u_{\text{ns}_i}(t)$, $\text{SPR}_i(t) = \text{SP}_i(t)$, and the setpoint tracking performances are maximized.

5. EXPERIMENTAL RESULTS

In this Section, the performances of the control architecture proposed in Section 4 are evaluated on the shrink tunnel workbench depicted in Fig. 1c. To do so, we discretize the TFs in (13), (15), and (21), and implement the corresponding lines of code in the software of the shrink tunnel microcontroller, which operates with the C programming language. Then, to analyze if each control specification is addressed, we carry out the following experiment. The shrink tunnel is turned on, starting from the ambient temperature, to assess the time required to reach a target temperature of 160°C (same for both zones). After that, several setpoint step changes are made, alternating between 150°C and 160°C , to analyze the tracking performances. We also include a brief machine shut down of roughly 5 minutes to evaluate the effectiveness of the implemented anti-windup strategy. Then, once the oven temperatures settle back at 160°C , the conveyor belt of the packs loop circuit is started, leading to the insertion of bottle packs inside the oven. After several minutes, the packs loop circuit is stopped to mimic the end of production.

To check if (S.1) and (S.3) are met, we compute the settling times during each setpoint tracking interval, which are defined as follows. Let $[t_A, t_B]$ be the time interval during which the setpoints are held constant at the value SP_{AB} , i.e. $\text{SP}_1(t) = \text{SP}_2(t) = \text{SP}_{\text{AB}}, \forall t \in [t_A, t_B]$. The settling time for the temperature $y_i(t)$, $i \in \{1, 2\}$, is defined as:

$$\sigma_i = \min_{\tau \in [t_A, t_B]} \frac{1}{60} \cdot [\tau - t_A] \quad [\text{min}] \quad (25)$$

$$\text{s.t. } \left\{ |\text{SP}_{\text{AB}} - y_i(t)| \leq 0.02 \cdot \text{SP}_{\text{AB}}, \forall t \geq \tau, t \in [t_A, t_B] \right\}.$$

Instead, for what concerns (S.2), we check if the deviations of $y_i(t)$ from $\text{SP}_i(t)$ are less than 5°C .

The PI controllers are tuned via (19) with $\varphi_{m_{\min}} = 70^\circ$ to minimize possible overshoots and/or temperature oscillations as well as favor energy saving, and $\omega_{c_{\max}} = 5.1 \cdot 10^{-3} \frac{\text{rad}}{\text{s}}$, associated with a minimum settling time of $\sigma_{\min} = 15 \text{ min}$, according to (S.1). Fig. 4 depicts the performances achieved by the proposed control architecture on the designed closed-loop experiment, highlighting the settling times $\sigma_i, i \in \{1, 2\}$, in (25) in each interval, and the deviations of $\mathbf{y}(t)$ from $\mathbf{SP}(t)$ when the packs are inserted into the oven. In any case, the σ_i 's achieved by the proposed control architecture are well below the requirements imposed by (S.1). During machine shutdown, the temperatures lower rapidly: in 5 minutes, zone 2 loses roughly 30°C . Once the shrink tunnel goes back to automatic mode, the proposed anti-windup strategy drives the temperatures towards the setpoint of 150°C in the shortest time possible (less than 20 min), effectively tackling (S.3). For what concerns the disturbance rejection performances in (S.2), the controller is severely impaired by the limited heating power of the heat resistors installed on the shrink tunnel under study. We can clearly see that $u_2(t) = 1$ (upper limit) during production. Even in this unfavorable condition, the controller is able to meet the $\pm 5^\circ\text{C}$ tolerance for most of the trial, with deviances greater than 5°C for just a few minutes. In any case, notice the smoothness of the control actions, favoring energy saving in (S.4).

6. CONCLUSIONS

In this work, we design the temperature controller for a shrink tunnel used in bottle packs manufacturing processes. In particular, we develop a model-based control architecture starting from a FOLPD model of the system under study, estimated from open-loop experiments. The proposed control architecture addresses several demanding specifications: setpoint tracking, disturbance rejection, maximizing the tracking performances after manual-automatic transitions, energy saving, and actuator limitations. Each specification is satisfied by the proposed centralized controller, which includes an inverted decoupler, one PI regulator per heating zone, and an adequate anti-windup strategy, which is the extension of the conditioned transfer AW algorithm (Peng et al. (1996)) to the MIMO case. The derived control architecture is experimentally validated on the shrink tunnel workbench at our disposal, proving the overall satisfaction of each control specification thanks to an ad hoc tuning rule for the PI regulators. Future work is devoted to designing a feedforward controller to improve disturbance rejection performances.

REFERENCES

Afroz, Z., Shafiullah, G., Urmee, T., and Higgins, G. (2018). Modeling techniques used in building hvac control systems: A review. *Renewable and sustainable energy reviews*, 83, 64–84.

Bai, J., Wang, S., and Zhang, X. (2008). Development of an adaptive smith predictor-based self-tuning pi controller for an hvac system in a test room. *Energy and Buildings*, 40(12), 2244–2252.

Garrido, J., Vázquez, F., and Morilla, F. (2011). An extended approach of inverted decoupling. *Journal of process control*, 21(1), 55–68.

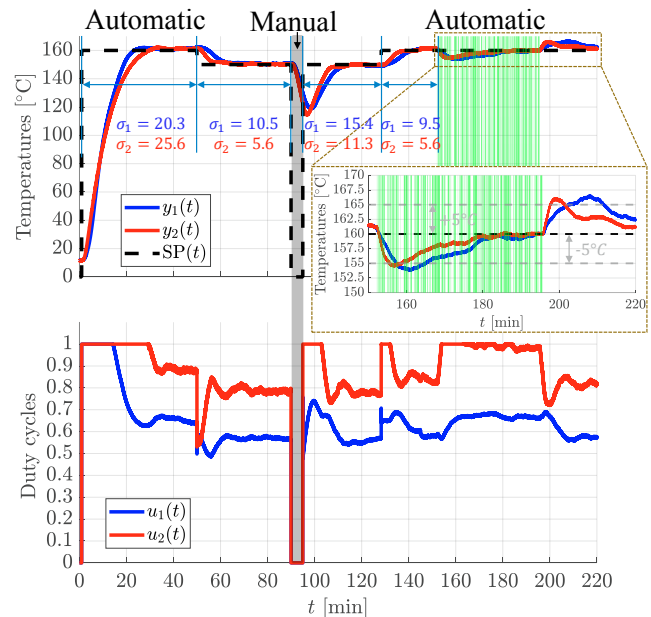


Fig. 4. Results achieved during the closed-loop experiment. The green vertical lines in the graph denote when $d(t) = 1$, i.e. when packs are inserted into the oven.

He, W., Xu, G., and Shen, R. (2014). Control of temperature uniformity in the temperature chamber with centrifugal acceleration. *Journal of Process Control*, 24(12), 1–6.

Hu, Y., Tan, C., Broughton, J., Roach, P.A., and Varga, L. (2018). Nonlinear dynamic simulation and control of large-scale reheating furnace operations using a zone method based model. *Applied Thermal Engineering*, 135, 41–53.

Ogata, K. (2010). *Modern control engineering*, volume 5. Prentice hall Upper Saddle River, NJ.

Peng, Y., Vrancic, D., and Hanus, R. (1996). Anti-windup, bumpless, and conditioned transfer techniques for pid controllers. *IEEE Control systems magazine*, 16(4), 48–57.

Rastegarpour, S., Gros, S., and Ferrarini, L. (2020). Mpc approaches for modulating air-to-water heat pumps in radiant-floor buildings. *Control Engineering Practice*, 95, 104209.

Ryckaert, V.G., Claes, J.E., and Van Impe, J.F. (1999). Model-based temperature control in ovens. *Journal of Food Engineering*, 39(1), 47–58.

Serale, G., Fiorentini, M., Capozzoli, A., Bernardini, D., and Bemporad, A. (2018). Model predictive control (mpc) for enhancing building and hvac system energy efficiency: Problem formulation, applications and opportunities. *Energies*, 11(3), 631.

Vasičkaninová, A., Bakošová, M., Mészáros, A., and Kleměš, J.J. (2011). Neural network predictive control of a heat exchanger. *Applied Thermal Engineering*, 31(13), 2094–2100.

Verhaegen, M. and Verdult, V. (2007). *Filtering and system identification: a least squares approach*. Cambridge University Press.

Zhang, R., Xue, A., and Gao, F. (2014). Temperature control of industrial coke furnace using novel state space model predictive control. *IEEE transactions on industrial informatics*, 10(4), 2084–2092.